2008 ASME Human Powered Vehicle Competition, Madison, WI

Design Report

Franklin W. Olin College of Engineering Pantas Human Powered Vehicle

Franklin W. Olin College of Engineering Human Powered Vehicle Team

Gavin Boggs, Giulia Fanti, Casey Canfield, Becky Belisle, David Stamp, Jonathan Raphael, Pamela Darvirris, Alex Jones, Alex Niswander…

3/22/2008

CONTENTS

ABSTRACT

The Olin College Human Powered Vehicle Team returns for its second year at the ASME HPV competition with the Vega. Our 2008 vehicle is a recumbent bicycle with a front wheel drive and steering system. The main goals during the design process were to maximize speed and control. To this end, we worked to improve steering stability, frame stiffness, aerodynamics of the fairing, and many other factors. We designed a more adjustable seat to accommodate many riders and provide more support and comfort. Our design decisions have been supported with much research into previous successful human powered vehicles.

Our 2008 vehicle is composed of entirely new parts. Many components have been significantly redesigned to optimize performance. With smaller wheels and shorter pedals, we have greatly reduced both frontal area and the length of the vehicle, for better aerodynamics and better maneuverability. Other geometries have been adjusted as well to improve performance, such as the seat back angle and ground clearance. Our fairing will also be greatly improved from last year's design, with great attention to construction feasibility, attachments, and visibility for the vehicle operator. We are confident that with these improvements our vehicle will be successful at the ASME competition.

1 DESIGN AND INNOVATION

Our design strategy this year was governed by a balance between focused component design and broader systems integration. We identified our primary subsystems as frame, fairing, drive train, and ergonomics. Starting with the basic dimensions of a rider, each team worked to optimize their subsystem to fit that rider within the scope of our team objectives. Most of these objectives were motivated by our participation in the single-rider speed challenge. In general, we tried to make design decisions that favor speed and rider safety. Moreover, we decided to make our vehicle more accessible to a wider range of team members by increasing adjustability and ensuring that the dimensions fit each team member who expressed interest in riding, whether competitively or otherwise. Some other primary design considerations were cost, both financial and in terms of time constraints. Ultimately, these latter factors ended up being the most restrictive on our design and played a very large part in shaping our final product.

1.1 FRAME DESIGN

The frame of the Pantas is an evolution of the frame developed last year for the Aurora, since we found that it suited our needs well. However, a number of improvements were implemented to make the vehicle more stable, more compact, stronger, and stiffer.

STABILITY

Our rider feedback from the competition last year called for a more stable steering geometry. We considered several factors which affect steering characteristics. These included wheelbase, the height of the center of mass, and rake and trail. In the design of bicycles, trail, the offset between the steering axis and contact point of the wheel, is generally considered the largest factor for determining steering characteristics. We decided to increase the trail from 1in to 1.5in in order to make the vehicle more dynamically stable at high speed and less responsive to errant steering. We also decided to raise the main tube to five inches off the ground; by raising our center of mass, we are effectively lowering the lean rate, thereby rendering the vehicle more stable [Fajans, Joel. Email Questions and Answers: Robot Bicycles. 2006,08-04].

COMPACTNESS

We made an effort to reduce the wheelbase of the vehicle in order to reduce our turning radius and improve control. To this end, we tried to reduce frame dimensions where possible; we shortened the length of the main tube and used 16 inch wheels both in the front and the rear. This allowed the rear wheel to be moved forward under the rider's back.

STIFFNESS

The Aurora's frame was quite flexible, which provided some suspension to absorb shocks and other system excitations, but was also detrimental to our fairing attachment; the flexibility required that the fairing have a sliding expansion joint. This year, one of our initial design goals was to fabricate a full composite fairing. A highly flexible frame in a rigid fairing would place great stress on the connection points, which could lead to failure of the connections or the fairing itself. For this reason, we made a concerted effort to improve the stiffness of the frame this year. To this end, we decided to use larger tubes for the main frame. Because the stiffness of a tube increases proportionally to the fourth power of radius, and weight is simply proportional to radius, larger tubes are very advantageous. A change in tube diameter from 1.5" to 1.75" increases the frame stiffness by 85% while adding only 17% to the weight. The theoretical limit to this improvement occurs when the walls become thin enough relative to the radius that wall buckling becomes a concern. However, our choice was based on a limited need for extra stiffness - using tubing larger than 1.75" would still have offered improvements in stiffness, but it would be overbuilding the frame. [need to support with design requirement – i.e. keep deflection below 0.5in]

We also reexamined our joint design and fabrication techniques based on suggestions given at the 2007 HPVC. Specifically, we considered two main options: mitered joints with internal support plates and brazed joints. The brazing process entails melting brass and using it to form a fillet between two separate pieces of metal, as opposed to welding where the fillet and tubes effectively become one piece of metal. Since brass melts at a lower temperature than steel, the metal faces much less extreme heat gradients, so the grain in each of the resultant pieces is more regular and remains the proper size. Welding, on the other hand, experiences much higher heat gradients during fabrication, so grain size is often irregular and consequently potentially subject to brittleness when compared to the heat-treated metal tube. While brass has a lower yield point than steel, the larger size of the fillet would theoretically enable the brass to support similar loads to welding with lower stress concentrations. Nonetheless, we ultimately chose not to use brazing for a variety of reasons. Our team already has several experienced welders, and the process of training members to braze well would represent a significant time investment. [weak argument - brazing is really easy - we should have an engineering reason for this choice] This is reinforced by the fact that welding has served our purposes well in the past as a structurally sound method for fabricating joints.

The stiffness of our frame is largely dependent on the strength of our frame joints. This is a function of many factors, including the joint style and quality of welds. In order to choose the most appropriate joint style for our frame, we considered three possibilities: a corner joint, a miter joint, and a plated miter joint (i.e. miter with a thin metal plate aligned along the plane of the joint). Based on our investigations, we decided to build our frame with a plated miter joint. We will now discuss the analysis and testing involved in this decision.

1.2 DRIVETRAIN

The drivetrain of the human powered vehicle is responsible for transferring power from the pedals to the wheels. Any inefficiency there will impede the speed of the vehicle.

In reviewing our drivetrain from the previous design iteration, we found it lacking in several areas. The largest problem we found to be the tendency of the chain to skip from one gear to another. Also, however, we faced issues with the fork chain rubbing both against the front chain and the wheel itself. In the process of fixing these two issues, we also managed to move the chainline to a more optimal path, reducing linear travel during angular misalignment.

Chain skip happens when the chain skips between one gear and another, either due to improper tuning or chain misalignment. This was the largest issue with our drivetrain – during turns this phenomenon would take place, wasting energy and frustrating our riders, especially during turns. In order to eliminate chain skip, we switched from a derailleur-based shifting system to an internally geared hub. Although this improvement allows for a variety of other optimizations, by itself it also solves the issues of chain skip.

An internally geared hub eliminates chain skip by reducing the number of sprockets to one. Modern derailleur systems are engineered for bicycles, and include features that enable the chain to switch gears more readily. Under controlled circumstances, where the chain path is very well controlled, this enables quicker shifting. However, for our application, where misalignment is a normal course of riding, this means that smaller angle turns cause chain skip to happen. The gears on an internally geared hub, however, are a more simple shape which functions better at keeping the chain in place.

Chain skip is also encouraged by the derailleur. The derailleur is held in place by a pull cable, pre-tensioned by a spring. This spring tension is strong enough to eliminate backlash in the shifting system and keep the derailleur in place under normal riding conditions, but not much stronger. It's restoring force is not great enough to keep the chain in the proper space. When we switched to an internally geared hub, we used a purpose built chain tensioner. The design of this allows us to very precisely define the plane which the tensioner swings in, ensuring it always directs the chain onto the gear.

Switching from a derailleur system gave us a large advantage in terms of our ability to define a particular chain path. In a derailleur, there is a wide area of space the chain could occupy, depending on which gear it is in. The most important constraint is that the drivetrain work in all gears, it does not work particularly well in any particular gear. Having only one gear with a fixed location, relative to the fork, allows us to accurately model and place the chain path.

The ideal chain path would place the drive side of the chain as close to the steering axis as possible, while maintaining clearances to prevent the chain from scraping the fork and frame. Moving the chain close to the steering axis is beneficial because it restricts chain misalignment to axial twisting, as opposed to a linear offset. While chains are not built to accept either, in practice cogs allow chain systems to function with some degree of each. For a given angel of turn, the angular misalignment is constant, while the linear offset varies as the distance between the chain and steering axis, so reducing this distance makes our drivetrain function more smoothly in turns.

In order to move our chainline closer to the steering axis, we used a raked fork. Rake is defined as perpendicular offset of the steering axis, and is most often used to control the trail and other steering properties of a bicycle. However, the exact interaction between rake, trail, and bicycle stability is poorly understood. Bicycle manufacturers rely primarily on precedence and intuition when determining these variables for their vehicles. Therefore, we used a limited amount of rake in our design, and controlled the trail by altering the steering axis angle.

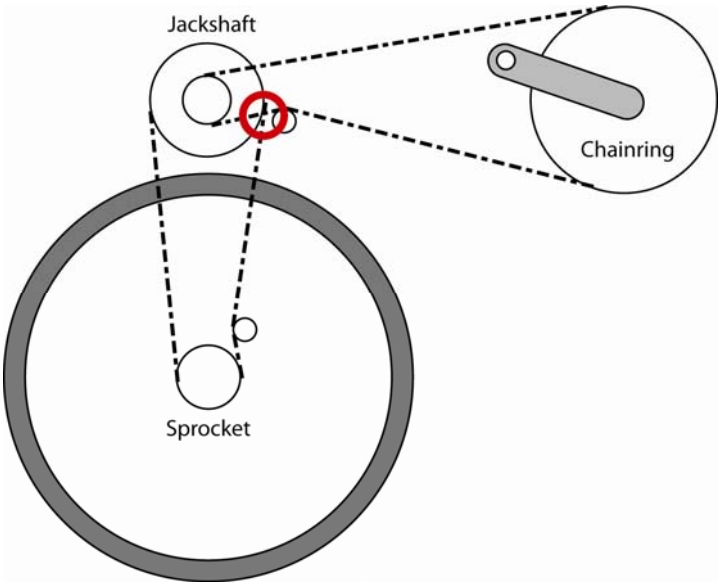

Figure 1. Red circle indicates region of chain interference.

Our design last year featured two types of chain rub. During sharp left turns, the fork chain and front chain would rub against one another. In order to fix this, we took several measures. The first was to use spacers to offset the front chain towards the frame of the vehicle. This increased the distance between the chains, thereby making it more difficult for the chains to travel the distance and intersect. It also has the advantage of leaving more space between the chains, easing mechanical work on the bike, which, it is hoped, will result in shorter pit repairs.

Second, we lengthened the front chain and moved the tensioner back, so that the chain leaves the interchange at horizontal. This moves the intersection point upwards, to where angular misalignment produces less of a linear movement, further reducing the ability for the chains to intersect. Since roller chains only experience friction al losses during articulation between straight and curved paths, this will not results in higher chain losses.

Finally, adding the chain tensioner, as opposed to the derailleur also improved this, by reducing the offset of the return chain path from the fork. This lets the chain stay on the gear of the interchange for more of its path, lowering the point at which it leaves the gear and thus where it starts to offset itself.

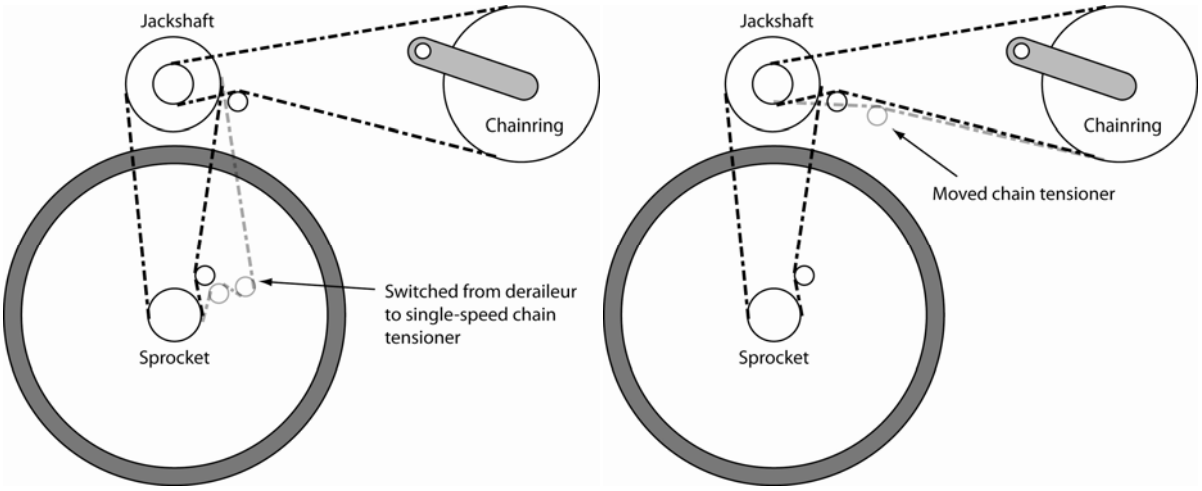

Figure 2. Chain line improvements: black path shows improvements over last year's chain path, shown in gray.

A potential downside to our choice of shifting transmission this year is the increased friction associated with internally geared drive systems. In a derailleur system, the only losses are frictional losses when the roller chains articulate – these are extraordinarily small. With a planetary gearing system, the various ring and planet gears are all always rotating, regardless of whether they are engaged at that particular moment or not. This additional movement results in additional frictional losses, potentially resulting in a less efficient drive system. We believe this loss is minimal, resulting in a fraction of a mile per hour in top speed in a straight course. Furthermore, by reducing chain rub and chain skip, we believe we have decreased friction there. All of these are of course overshadowed by the mechanical trouble and time spent with a broken drive train. All other considerations pale when compared to reducing our down time during races.

1.3 Fairing Design

For this year one of our main goals was to bring a fully faired HPV to competition. Although we had designed and modeled several fairings, we did not have the budget or time to manufacture our final design during the previous year. Taking the previous year into consideration we broke our fairing team into two groups: design and manufacturing.

For the initial design phase of the fairing, the design team developed several SolidWorks models to compare the pros and cons of different fairing features. These features included canopies, nosecone shapes, and tail shapes. By analyzing these SolidWorks models in Cosmos FlowWorks we developed an idea about how these features affected the aerodynamics of the fairing. With this analysis in mind we decided to manufacture a fairing without a canopy, since every model with a canopy generated significantly more drag than our non-canopy models.

The next step in our fairing design consisted mainly of finding resources on fairing design, and studying aerodynamics. One particularly interesting method of designing fairings we found involved stacking airfoils. By using airfoils that are known to generate low drag, we were confident that we could design a fairing with a low C_dA which could fit any of our riders. With further research, we decided that series 6 NACA airfoils would not only provide the low drag that we required, but also the flexibility to easily vary the shape of the fairing. The initial design based on series 6 NACA airfoils was generated and analyzed with Cosmos FlowWorks. The results were very promising, but there were still some problems with this design.

In order to get NACA airfoils to fit a rider, they had to be at least ten feet long. This would outline a fairing which was much longer than we could manufacture and would be much heavier than we wanted. In order to compensate for this, we scaled the airfoils to fit a human being, and also be short enough to be feasible for manufacturing. The new fairing differed slightly from the original NACA airfoil design, and so we did analysis on the final shape to ensure we had not lost any aerodynamic advantage.

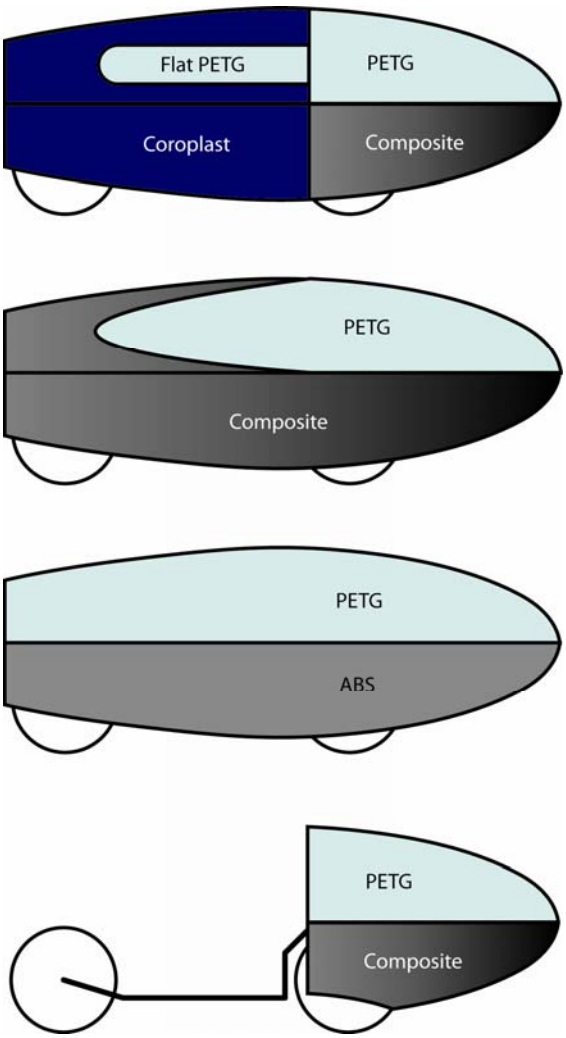

Figure 3. Fairing construction options.

While the manufacturing team had little work to do during the initial fairing ideation, as soon as we had settled on the stacked airfoil design, they began looking into materials and methods for making our fairing design a reality. The first idea for building a fairing with this shape was to use fiberglass or carbon fiber. The difficulty of using both of these methods comes from manufacturing the plug and importantly, the mold, for laying up fiberglass. After careful consideration of this tedious process and our budget we determined that carbon fiber would be much too expensive to use for the entire length of the fairing.

Next, we looked into using thermoforming. This technique would allow us to not only create a plastic shell which was very close to the shape of the desired fairing, but also create a clear window which fits the curve of the fairing. In order to thermoform a shape this large we searched for companies around the Boston area with the ability to

thermoform shapes over 6 feet. One company, Mayfield Plastics, agreed to provide the labor and means to create our fairing. Unfortunately their thermoforming machine does not have the capability to manufacture our full fairing. Due to this we decided to make our fairing out of a mix of thermoplastic and fiberglass. The thermoformed plastic will cover the front half of the fairing and provide us with a substantial window. The back half of the fairing will be composed of fiberglass, and provide a lightweight and strong tail.

1.4 Steering Design

We had two main goals in designing the steering mechanism this year. First, we wanted to make sure that small displacements of the wheel would be corrected by the restoring force of the rake and trail. This would increase our stability; accordingly, we increased our trail by 0.5in. We also wanted a steering mechanism that was well-coupled to the wheel axis, so that even small displacements of the wheel would be translated into motion in the handlebars.

We first considered a worm gear-spur gear steering mechanism. This design would control the motion of the wheel very well, but had two main problems. Using a worm gear would greatly increase the gear ratio of handlebar motion to wheel motion. While this increases our control; too high a ratio would make sudden turns difficult to execute. The other problem is that a worm gear would require us to significantly rotate the handlebar axis, much like a car rather than a bike. This would make leaning into turns difficult, which is integral to attaining a small turning radius.

Another facet of the steering that required optimization is the two-bar linkage control mechanism. After utilizing a two-bar design last year and experiencing success, we decided to iterate and optimize the design. A problem we ran into last year was that the steering became hard to control on steep turns. This is an effect of the moment arm shrinking as the wheel angle increases. One solution we examined was offsetting the tie rods from the handlebar and wheel axes. By carefully choosing the offset, we could maintain a roughly constant torque throughout our expected range of wheel angle.

1.5 Ergonomics

Seat

The goal of our set is provide support and comfort the rider to help them maintain a position that allows for maximum power while minimizing the height of the bike. The seat angle was obtained by allowing the line of sight to reach just above the knees. This minimal seat height will be possible with greater visibility this year due to the use of a large thermoformed window as part of the fairing. In order to make this position comfortable, we paid careful attention to supporting the rider's head. We believe proper support of the rider's body will allow them to efficiently transfer power while pedaling in the position which minimizes frontal area for aerodynamics.

Another important aspect of the seat is the ability to quickly accommodate riders of different sizes. Last year's design required loosening and tightening hose clamps at every rider change. To facilitate faster rider changes this semester, we will use a car seat slider to make quick and reliable seat adjustments.

Foot Path Design

The pedal path also received some revamping during the design phase. The goal is to make the motion as natural and fluid as possible, increasing the efficiency of pedaling. In the 2007 bicycle design the foot path interfered with

the line of vision, causing limited visibility. This year's design increases rider visibility without sacrificing foot path ergonomics. With this improved foot path steering accuracy will be improved. [discuss shorter cranks, narrower Q factor]

HAND/WRIST POSITION DESIGN

The last area of ergonomic interest was in the hand and wrist position on the handlebars. The handlebars are positioned with the grips vertically to keep the hands in an ergonomically pleasing position. This was found to be the most comfortable position for steering accuracy and rider comfort. When skiing and driving the same hand position is used, as the palms face inward instead of down, helping with control and reducing arm tension to a minimum.

According to several riders, a steering position with vertical bars is much more comfortable than a horizontal system. They indicated that steering in this fashion would promote smoother hand motion when turning corners. The handlebars respond easily to the touch and do not require any uncomfortable movements to initiate or continue turns. Though there were not any major issues with the steering system last year, these current improvements are a great contribution to the design.

ROLL BAR DESIGN

For our roll bar, we planned to use composites rather than steel in order to decrease weight and improve ease of curve-fitting. Since we do not have a tube bender, fiberglass will enable us to create a curved profile, which is better in terms of both material efficiency and even load distribution. We are using the results of basic composites research to determine what the composition of the roll bar needed to be in order to match the strength of steel.

The roll bar was fabricated with both carbon and fiberglass, a total of three layers. We used a five ounce ply of fiberglass, a two ounce ply of carbon fiber, and finished with a one ounce ply of fiberglass. These were laid up on a foam cylinder bent into the correct geometry and mounted onto steel tubes. The tubes will be bolted onto the frame behind the car slider.

2 ANALYSIS

2.1 FRAME ANALYSIS

During computational analysis of the frame for the 2007 HPVC, we noticed that the stresses at the joints were largely dependent on the moment load on the joint, and that reducing this loading would be an important step to relieving stresses at a particular joint. A simple optimization would be impractical, because the frame geometry sits at the intersection of several competing interests. Therefore, we chose to create a simulation that varied several key parameters, in order to better quantify the effect of altering our frame geometry on the loads at our critical joint, and the frame stiffness as a whole.

Several assumptions and simplifications were made for our analysis. We assumed that, for various values of the wheelbase, the center of mass of a rider was stationary with respect to the front wheel. For investigating different elevation angles of the seat, we assumed the center of mass to rotate about the rider's crotch. This point was determined experimentally.

We began our analysis by writing a script to calculate stresses on our critical joint, given certain critical geometric parameters and accelerations. To simplify our analysis, all masses were considered as point masses. Superposition

was then applied, combining all input masses into a single point mass. The given accelerations were applied, and a moment calculated about the front wheel. This moment was used to calculate the vertical reaction at the rear wheel; the vertical and horizontal reactions at the front wheel were then determined. We assumed our vehicle to maintain front-only brakes, which also results in a statically determinant system.

Our results are shown in the following graphs. While we varied the wheelbase, we assumed a seat angle of 30 degrees from horizontal; when we varied the seat angle, we assumed a wheelbase of 60 in. All plotted results are normalized about this point, which was chosen because it was a nice number that approximated our initial frame designs.

All analysis was done with two acceleration cases-one with normal acceleration, one that assumed a 3G bump. This was done to determine whether or not different loading cases would invalidate our results.

Our results indicate that shortening the wheelbase will have beneficial effects on our frame, although it follows the laws of diminishing returns, and a given decrease does less to reduce the moment as the wheelbase becomes shorter.

In order to gauge the efficacy of each joint, we conducted finite element analysis on each of the three options using COSMOSWorks. We decided to model the main weight-bearing joint, located between the main tube and the up tube. Loading conditions were calculated based on a 200 lb rider experiencing a 3g bump as well as deceleration from 20 to 0 mph in 10 feet. These conditions were calculated for our prototype frame, which is lightly different from the final frame geometry. As such, the loading conditions would also be a little bit different. We plan to modify our analysis results to reflect these new loading conditions. We applied these loading conditions at a point 4 inches away from the joint. The following diagrams illustrate the Von Mises stress distribution for each model.

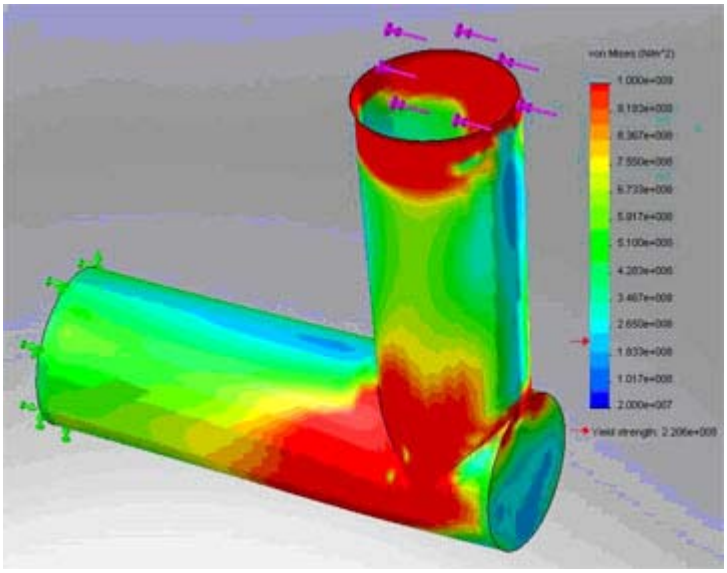

Figure 4. Corner Joint.

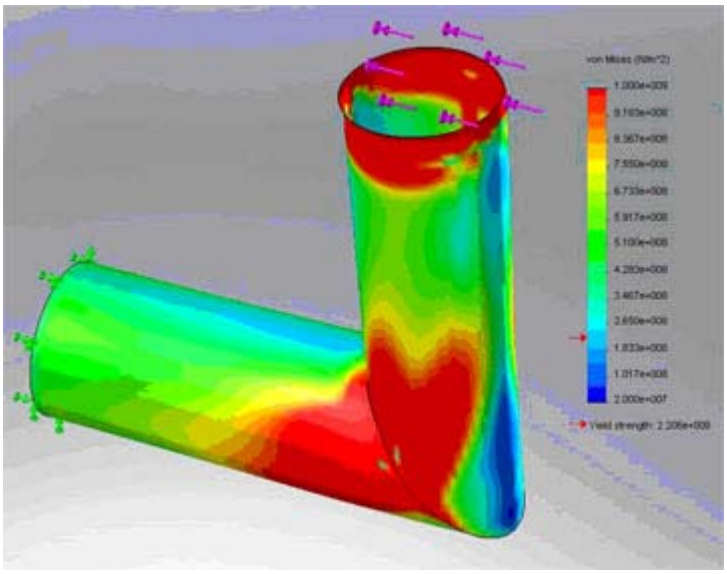

Figure 5. Miter Joint.

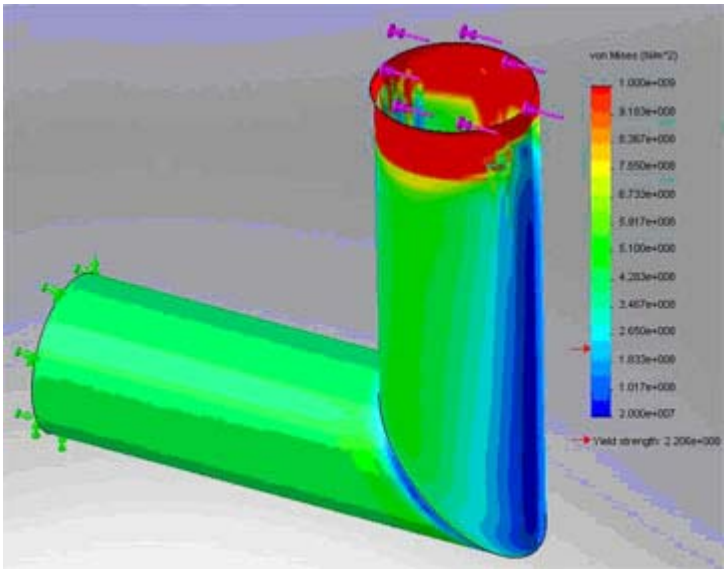

Figure 6. Miter joint with plate.

These results indicate that the plated miter joint experiences the least stress; its maximum stress level at the joint differs from those of a normal miter by approximately one order of magnitude. We recognize that stress levels appear to be extremely high at the surface where the load is applied, but this is most likely due to the fact that we modeled the joints as surface elements with very little depth. This presumably results in edge effects that would not be an issue if we were to model the joints in terms of solid elements. We could not test this hypothesis because of computational limitations. The inner plate of the rightmost joint is represented as a surface with little to no thickness, as this adequately reflects the joint geometry while still modeling inner stress. Here we can see more detailed, rescaled views of the stress distribution on the plated miter joint.

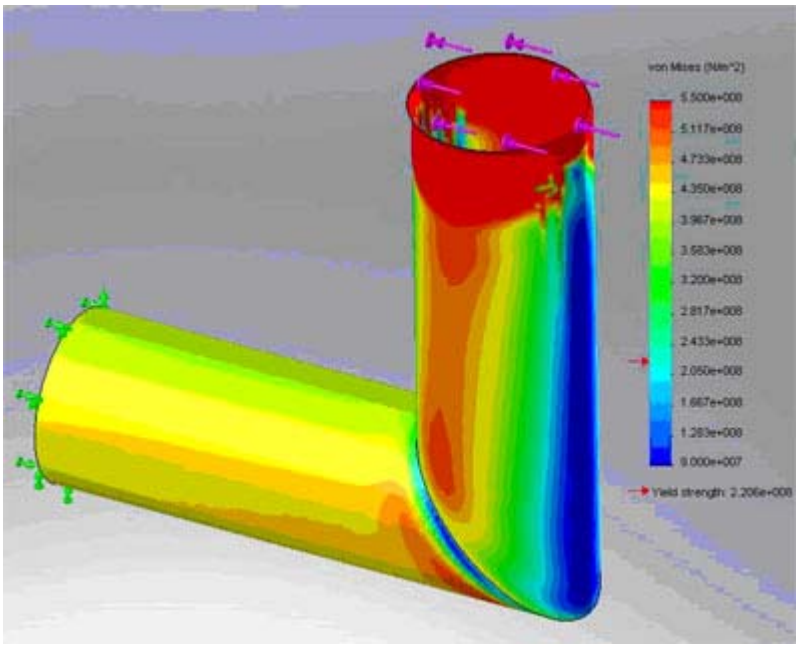

Figure 7. Side view of plated miter joint.

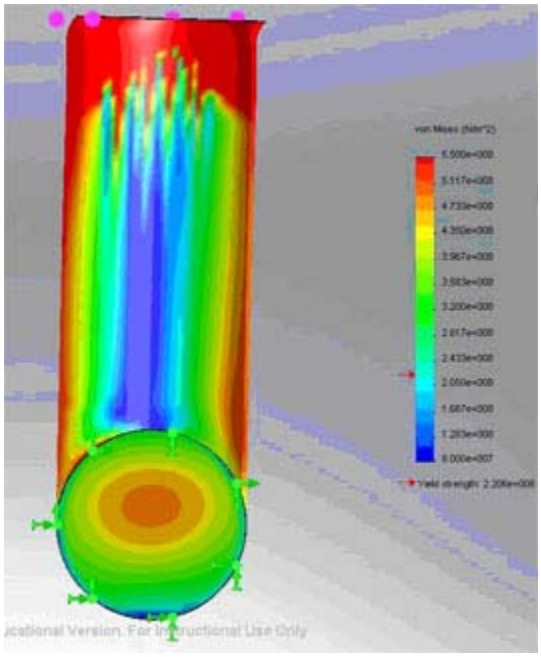

Figure 8. Front view of plated miter joint.

From this figure, we conclude that the highest stress concentrations in the joint appear to be transferred to the interior plate. This is optimal, as fortification of the interior plate is a relatively easy process. However, we also note that the stresses at the joint are well above the yield stress. For this reason, it may be necessary to utilize gussets at the joints. Alternately, we can also use tubing with larger diameter and/or larger wall thickness. However, we also recognize that our computational results may not be completely accurate, since we temporarily

used an unfortified corner joint on our vehicle last year without significant problems. This may be due to the fact that our loading conditions for this analysis are stringent, and would probably not be met under regular riding conditions.

2.2 FARING ANALYSIS

To begin our analysis for this year, we compared our new design based on NACA airfoils to that of last year's minimal curvature design. To do this comparison, we used COSMOS FLOWORKS to calculate the and visualize the pressure gradient around each fairing. These examinations were performed at a constant Reynolds's Number of 3898000, since both fairings had approximately the same length in order to fit the rider and a wind speed of 17.88m/s (approximately 40mph). Looking at the pressure gradients for both designs we noticed that last year's model had a maximum pressure of 101515Pa and that there is a sudden drop in pressure as air rises over the front half of the model. In comparison, this year's design has a maximum pressure of 101554Pa and the air gradually drops in pressure as it rises over the fairing and peaks at the center of the model. By examining the force felt by the fairings in opposition to the wind speed we were able to calculate their respective s. The for the minimal curvature design was 0.021m² while airfoil inspired fairing has a of 0.014m². This marks a 1.5 improvement in over last year's design.

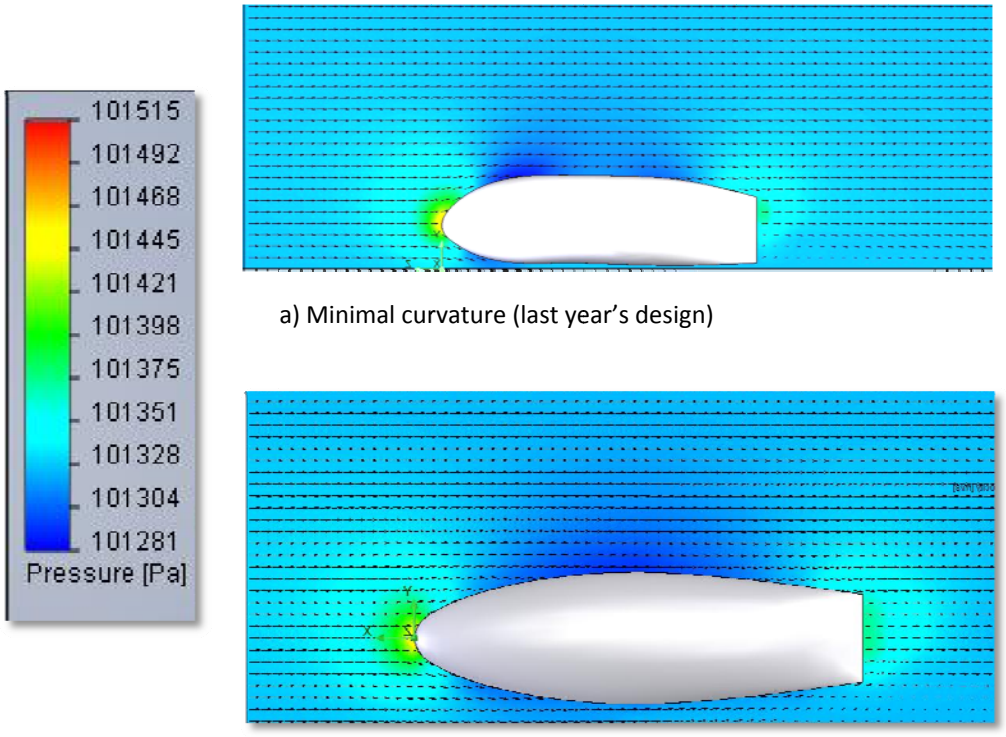

a) Minimal curvature (last year's design)

b) Airfoil shape (this year's design)

Figure 9. Pressure gradients for fairing designs: a) Minimal curvature (Maximum Pressure: 101515Pa); b) Airfoil shape (Maximum Pressure: 101554Pa)

As well as trying to minimize with our design we hoped to minimize low pressure zones, keeping a relatively constant pressure over the surface of the fairing. Low pressure zones foster the air separation which results in wake drag. The airfoil shape experiences a greater drop in pressure (266Pa) than the minimal curvature design

(234Pa). However, the magnitudes of these drops in pressure are so small we don't think they will have any serious effects on drag.

Another important note is that we ignored the effects of the wheels on drags. We chose to ignore the wheels in these designs because we were looking at these models comparatively and the wheels would be in the same place for both models.

After examining these designs and determining that the airfoil inspired shape was an improvement over last year's design, we analyzed the benefits of narrowing our fairing. We took our original model and made it narrower while maintaining the NACA airfoil shape. We then compared this modified airfoil design to our previous model using the same flow conditions as described earlier.

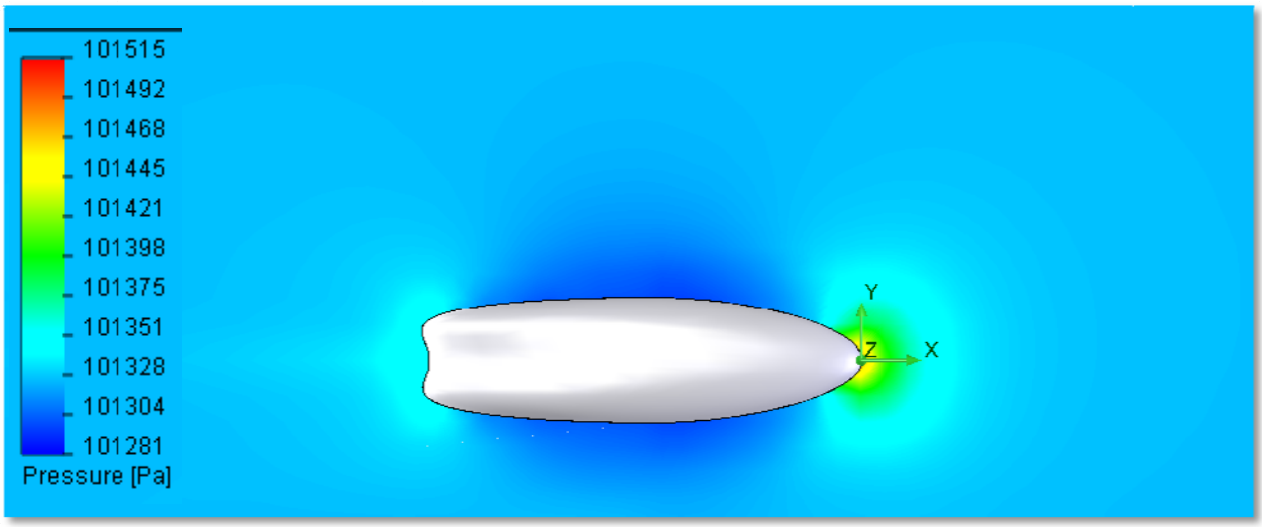

Figure 10. Pressure gradient for modified airfoil design. Maximum Pressure: 101697Pa.

2.3 Controls Analysis

To frame the problem, we created a mathematical model to optimize the offset distance between the tie rod connections and the center of rotation. An idealized turning situation would involve the rider applying a constant torque to the handlebars and receiving a linear turn response. The vehicle with these modifications would be easier to control, and the rider would have to exert less effort to turn.

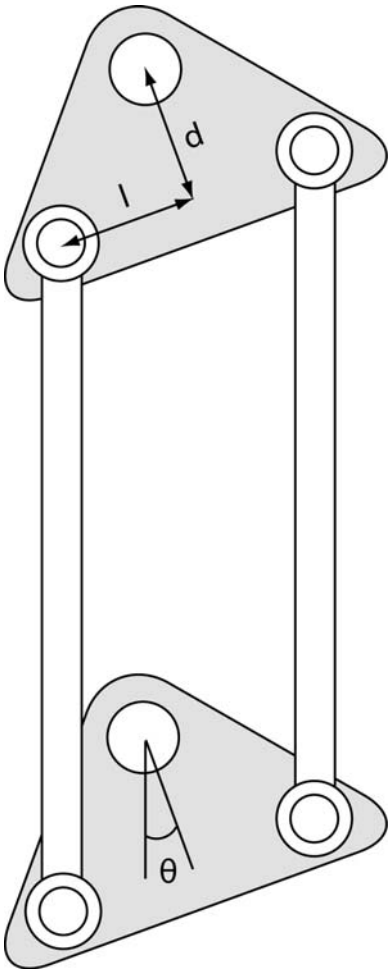

Figure 11. Diagram of offset steering geometry.

We set up the model as shown in the figure above and attempted to find the torque produced when forces F_1 and F_2 are applied to the handlebars. Solving the kinematics resulted in an equation relating torque to the applied forces:

$$\tau = (F_1 - F_2)dsin(\theta) + (F_1 + F_2)Lcos(\theta)$$

This equation indicates that the offset affects the torque produced when the force exerted on each handlebar is different. If the forces are the same, the first term cancels and the torque produced is independent of the offset.

2.4 Vibration Analysis

One issue that we did not consider explicitly during the design phase but that will ultimately be relevant for our purposes is the harmonic response of our vehicle. That is, as our vehicle is excited at certain frequencies, we would like to see what kind of response it exhibits. To predict this, we conducted modal analysis in COSMOS Works to find the fundamental frequencies of the frame. We modeled the components of the frame as beam elements and obtained the following results.

Mode No.	**Frequency(Hertz)**

1	0.008261
2	0.004111
3	0.000162
4	0.000496
5	0.001189
6	0.014287
7	85.285
8	89.779
9	198.24
10	338.06
11	362.37
12	699
13	717.45
14	893.81

Figure 12. Table of frequency response results for our frame.

We chose to consider only frequencies above the 7th mode number, as frequencies below 1 Hz are not really relevant for our purposes. Moreover, for each relevant frequency, we can visualize the mode shapes to determine how the frame will vibrate. An example of this can be seen in the figure below. We find that the fundamental frequencies do not all excite the system in the same plane; this means that in our efforts to increase stiffness, we should have also considered multiple axes of flexing. However, we did not have problems with this last year, and the fact that we increased our tubing diameter this year should mitigate the effects of a problem that is effectively negligible.

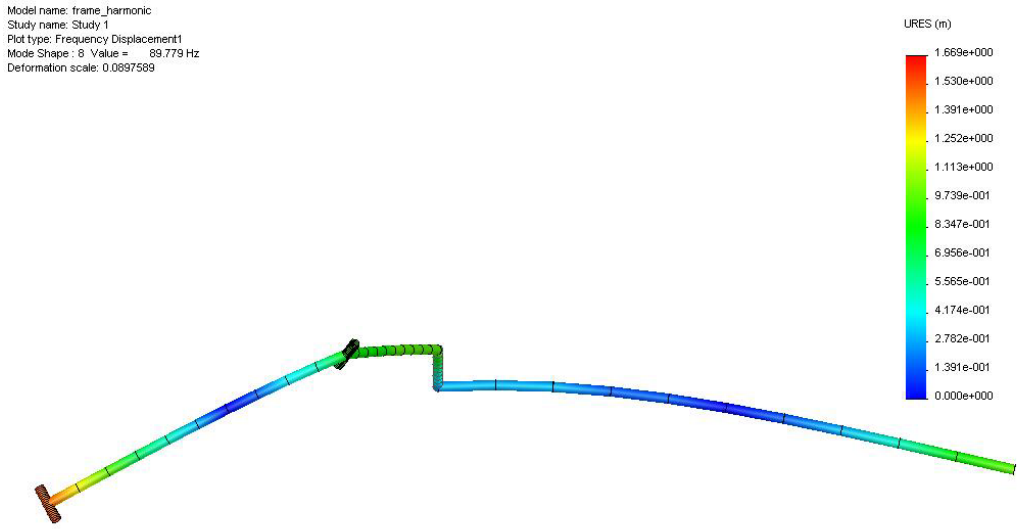

Figure 13. Mode shape for fundamental excitation frequency of 90 Hz. The flexing is out of plane of the frame.

The more important result of our modal frame analysis is that it gives us a method for evaluating the validity of our frame model. We plan to experimentally conduct modal analysis on the frame, which will allow us to compare fundamental frequencies between our model and our actual frame.

2.5 Roll Bar Analysis

In order to best maximize space, we made the shape of the roll bar fit around the shape of the fairing near the shoulders of the rider. This decision was made with the confidence that a suitable composition of composites could be found to meet the strength specifications. [composites research results]

To analyze our design we modeled the geometry in Solidworks. We applied a 485lb force 8 degrees, as required by the competition rules, from the vertical to the top of the arch. Since the specification comparison involved the strength of steel, we set the material of the arch to plain carbon steel. The Von Mises stress is shown in the figure below.

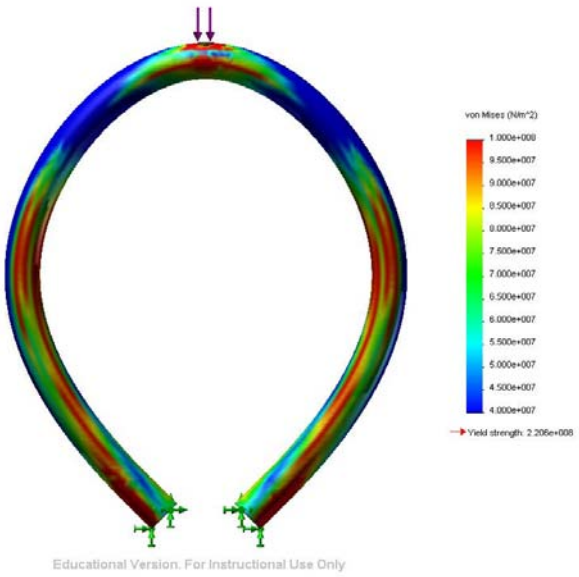

Figure 14. COSMOSWorks output for loading of roll bar.

As can be seen, the yield strength of the steel is higher than the maximum stress, indicating that the roll bar will hold up structurally under physical testing. Since the composites have a comparable tensile strength with that of steel, we are confident that the roll bar will meet the safety standards set by ASME.

3 Testing

In order to validate our analysis, we conducted a range of tests on various components and structures, as well as our vehicle as a whole.

3.1 Joint Testing

Test samples were created with three different styles of welded joints: a plain miter joint, a miter joint with an internal plate, and a corner joint with an open end. Each piece was tested in compression in the Instron Universal Materials Tester with one end abutted against the top compression plate and one end supported by a pin in the support shown in Figure 1 so that it could freely rotate. The entire setup can be seen in Figure 2. The samples were all sized with 4 inches between the contact point with the compression plate and the far edge of the joint. Each sample piece was compressed past both the yield and maximum loads.

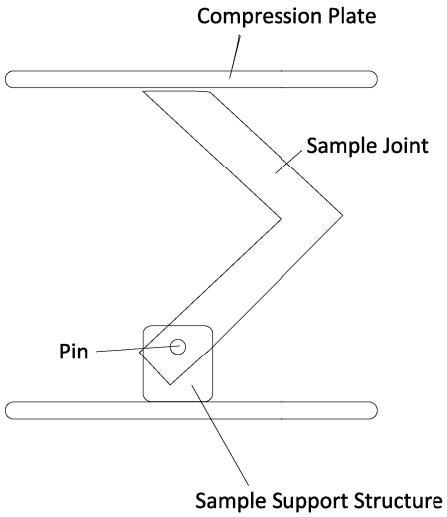

Figure 15. Compression Test Setup.

RESULTS

Failure in each case was caused by the buckling of material around the joint. These points are indicated by red circles in the following photographs.

For the miter joints, the yield load appears to be at approximately the same extension of 4 mm, while the yield load for the open corner joint is at approximately 2.5 mm. The maximum loads follow the same pattern. However, the yield load and maximum load for the open miter joint are significantly lower than those for the internal plate miter joint and the open corner joint. The internal plate miter joint seems significantly stronger than the open corner joint as well, with a maximum load of over 6000 N.

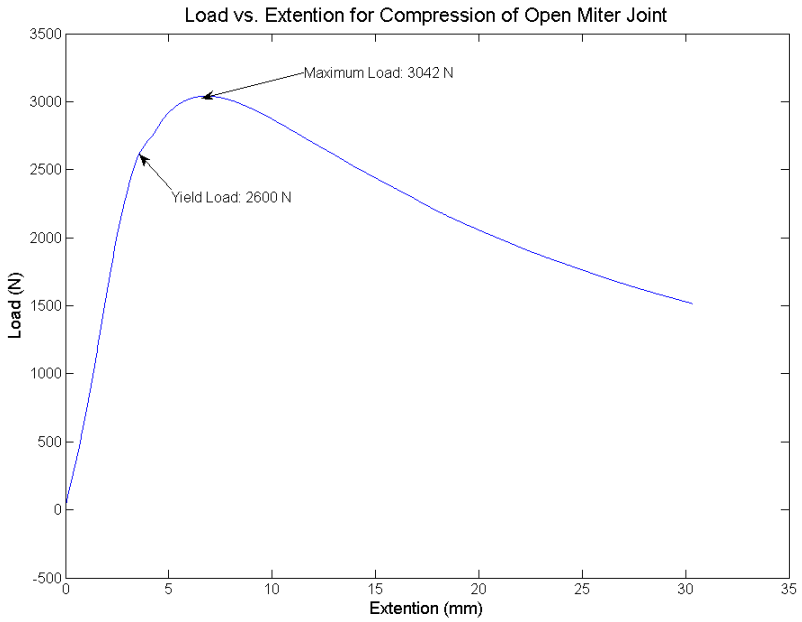

Figure 16. Load extension graph for the open miter joint. Yield load is at 2600 N and maximum load is at 3042 N.

Figure 17. Photograph of open miter joint after testing. The two buckling points are circled in red.

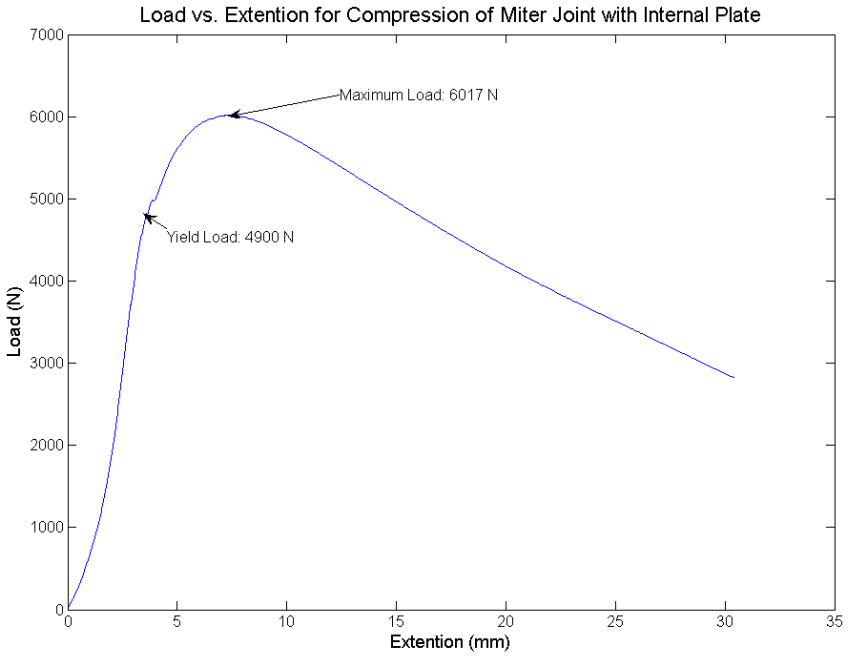

Figure 18. Load extension graph for the miter joint with an internal plate. Yield load is at 4900 N and maximum load is at 6017 N.

Figure 19. Photograph of miter joint with plate after testing. The buckling points appear to be more even.

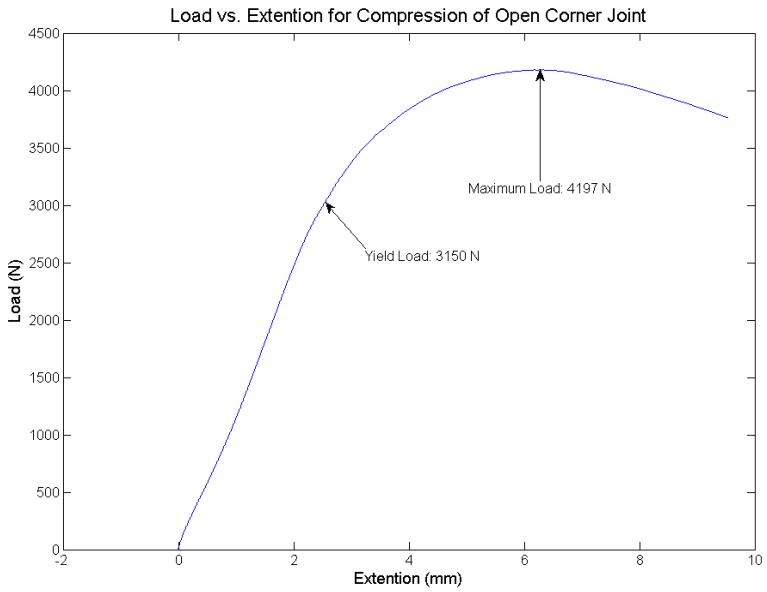

Figure 20. Load extension graph for the open corner joint. Yield load is at 3150 N and maximum load is at 4197 N.

Figure 21. Photograph of the open corner joint after testing, with the buckling point circled in red.

Recommendation

The miter joint with an internal plate has both the highest yield load and the highest maximum load, and thus seems to be the best choice for joint construction.

3.2 Composites Testing

Introduction

This experiment aimed to quantify the relative strengths of a variety of weight, weave and ply combinations in simple composites that could plausibly be used to construct a bicycle fairing. Both carbon fiber and fiberglass composites were tested, in addition to fiberglass-carbon hybrids. The experiment resulted in an excellent mass estimation tool, in addition to a significant amount of composites experience and qualitative information.

Experimental Procedure

We created dog bones to test on an Instron Universal Testing machine. These were created in a variety of different fabric combinations - we tried to test a representative sample of anything that might end up being used for fairing construction. The dog bones we created were made to ASME materials testing specifications. For larger areas, the only type of fabric used in this experiment that should exhibit directional behavior is the plain weave carbon. However, on such a small scale weave details become quite important, since it is easy to have a sample cut for which the skinny part of the dog bone falls between strong areas in the weave.

In general for this experiment there was not a significant trend towards weave dependent behavior, but there were definitely isolated samples that exhibit a split that could have been caused by something similar. Note 'Deviation #2' on the final graph - clearly a two/two split in samples, this could have been caused by an awkwardly angled weave pattern in the original sample. Many of the other outliers in the data could have been caused by these weave differences, amplified greatly because of the small scale.

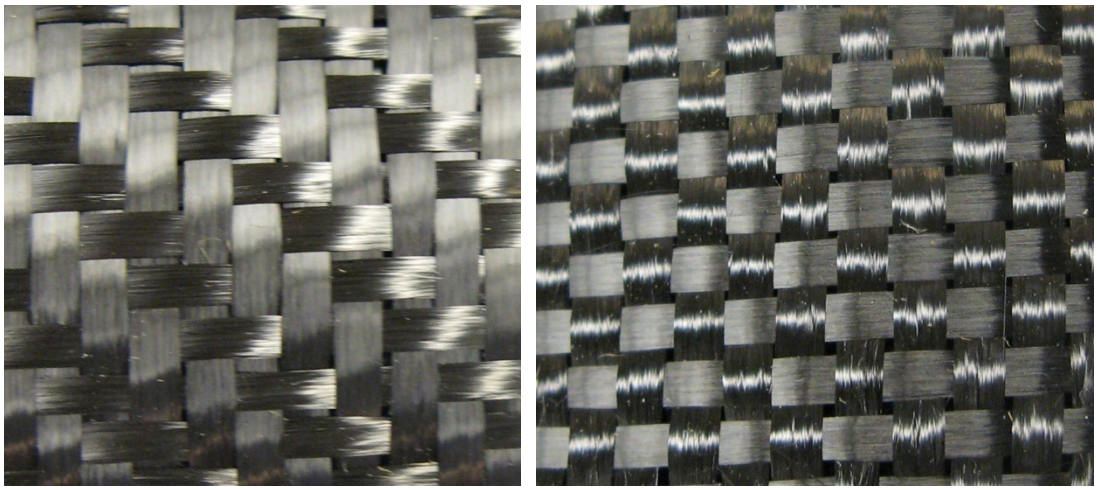

Figure 22. The above image shows a visual comparison between the two main types of carbon fiber weave. On the left is a plain weave (directional) while on the right is a twill weave (non-directional).

Data Analysis

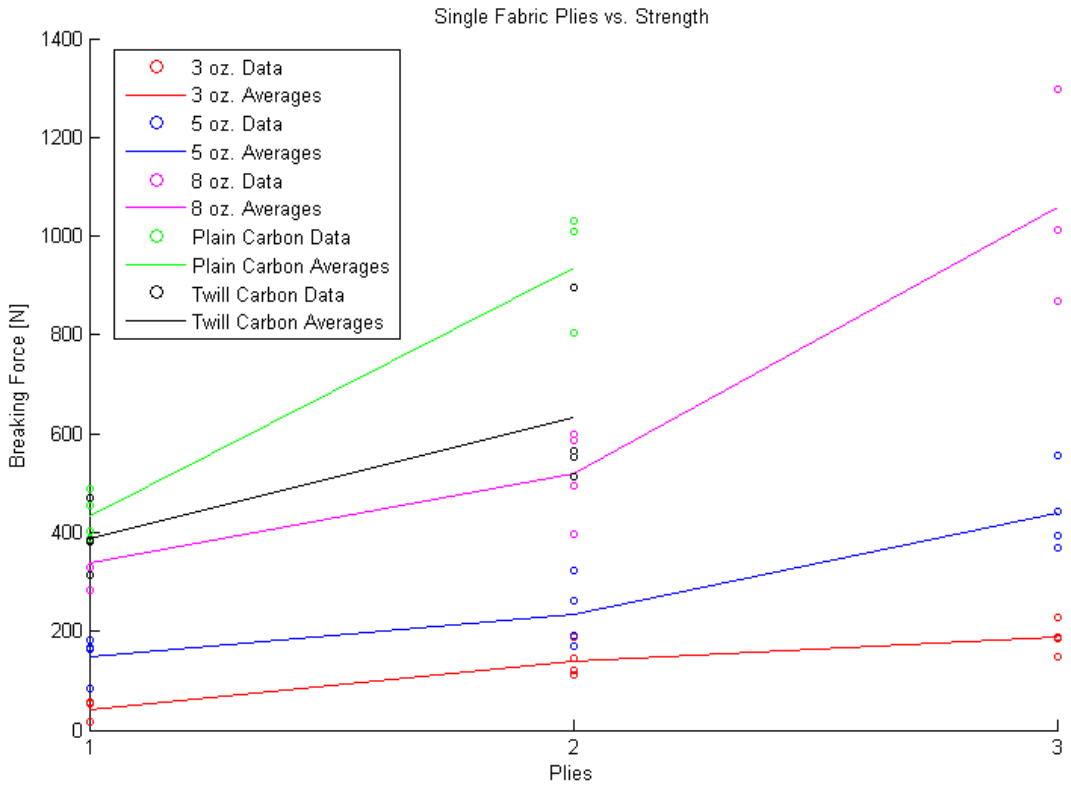

Figure 23. There is clearly a correlation between number of plies and strength of the resulting article. However, it does not seem like this correlation is always of the form $single\ ply\ strength \times number\ of\ plies\ =\ strength.$

As expected, the general trend in these results was always an increase in strength for every increase in the number of plies. In some cases, such as the 3 oz. cloth, 8 oz. cloth and the plain carbon weave, this addition was a relatively direct relation of the rough form $single\ ply\ strength \times number\ of\ plies\ =\ strength.$ For the other fabrics, the relative strength of each additional ply beyond the first was lessened, possibly because of errors introduced in the more complicated layup process.

Another goal of this experiment was to create a means for accurately estimating the eventual finished weight of composite pieces. Each finished set of identical pieces was massed after being destroyed, and these masses were used to find an average mass for the set. These resulting masses were plotted against the total fabric weight that went into the piece, and a linear relationship was found (as shown in the Figure below). A mathematical relationship between cumulative fabric weight, area, and finished part mass was then found, starting with the relationship from the graph below:

$$F = cumulative\ fabric\ weight$$

$$M = finished\ article\ mass$$

$$M = 0.031 \cdot F$$

$$A = area\ of\ article = 0.0004774184m2\ for\ a\ single\ sample$$

$$M = kAF = 0.465 = k \cdot 0.0004774184 \cdot 15.0$$

$$k = 64.9 \frac{g}{oz \cdot m^2}$$

Which gives the final relationship to be:

$$M = 64.9 \frac{g}{oz \cdot m^2} \cdot AF$$

Using a rough surface area, we can estimate the weight of a full fiberglass bike:

$$M = 64.9 \cdot 24 \cdot 4.89 = 7.6kg$$

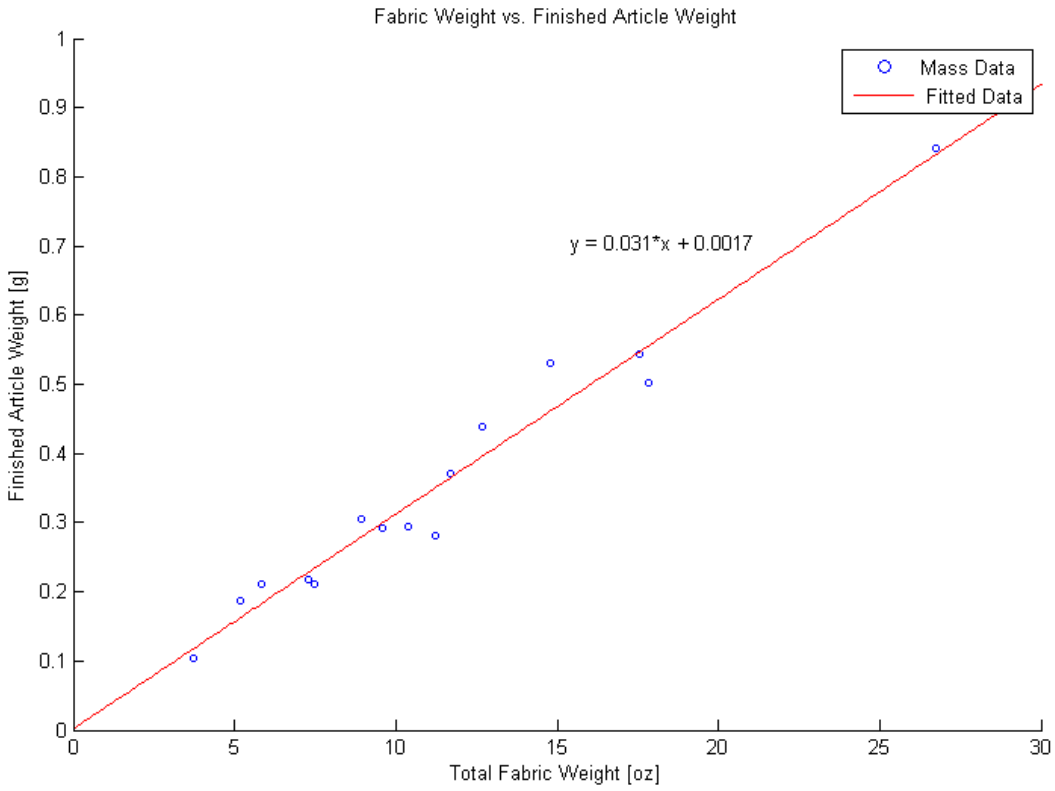

Figure 24. This figure shows the relationship between cumulative fabric weight and finished article weight. Cumulative fabric weight was found by adding the weight (in oz) of all the cloth used in the piece, while the finished article weight was found by simply massing the article on a scale.

Strength to weight performance was relatively as predicted, with the pure carbon samples coming out on top in most cases and the fiberglass-only samples generally near the bottom. There were a few major deviations from the expected. In 'Deviation #1' from the figure below, the weight of the sample seems to have been erroneously measured. The sample represented is a single ply of carbon cloth, and the weight is both drastically more than the other single ply carbon set and is even more than one of the two-ply carbon sets. The other major deviation ('Deviation #2') was most likely caused by a manufacturing defect, since both of the two failing samples were cut

from the same area of the original sheet. As expected, the fiberglass-only samples seem to be somewhat more consistent in strength to weight ratio, but the samples were (through observation) far less prone to manufacturing defects. Another notable observation was that the hybrid samples were in general not significantly stronger for their weight than the fiberglass-only samples. There were exceptions to this rule, though, such as in 'Deviation #3', which will be investigated for possible applications. The set of samples represented by 'Deviation #3' is the carbon twill / 8 oz fiberglass hybrid.

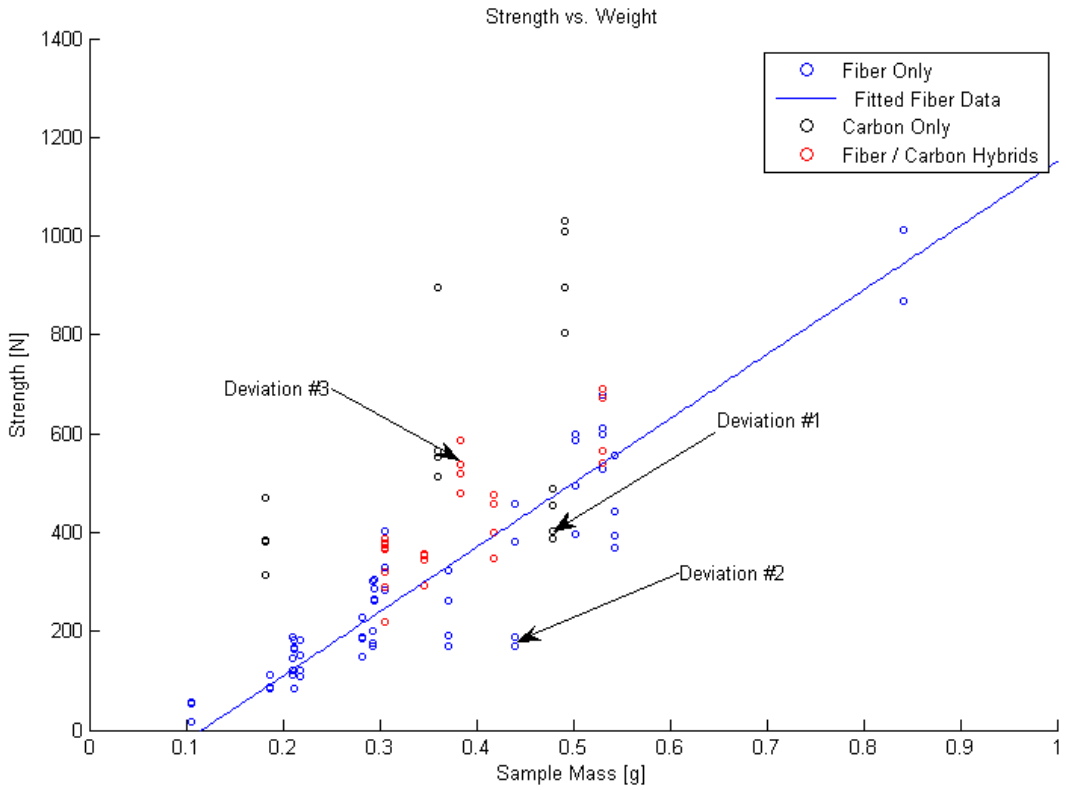

Figure 25. Note that many sample sets had one or even two significant outliers, probably caused by manufacturing defects or weave directionality.

CONCLUSION

This experiment was quite successful in collecting data that might be useful for design larger composite structures such as a bicycle fairing. Quite probably the most important result was the creation of a general rule for estimating weight of a completed piece. Other important results include data about the relationship between number and type of plies and the total strength of the finished piece, as well as data on strength to weight ratios of various fabric combinations. An important qualitative understanding of the technique and feel of composite construction was also gained.

3.3 WIND TUNNEL TESTING

We tested 1:11 scale models in a wind tunnel under a range of wind speeds and measured the resulting drag force. We were interested in testing our fairing designs with speeds up to our maximum predicted speed of 40

mph. However, due to the 1:11 scaling, this would equate to speeds of up to 440 mph inside the wind tunnel. However, the practical limitations our wind tunnel limited testing speeds to 98.43 mph. The modified airfoil results show marked improvement from the original revolved airfoil design, with an average difference of 2.5 N. The nose cone showed similar results to the revolved airfoil. The wind tunnel test for the nose cone neglects the affect of the remaining structure behind the bike, but it should provide sufficient aerodynamic shielding for the slower speeds of the endurance event.

Hertz	Wind Speed (MPH)	Nose Cone Drag Force (N)	Revolved Airfoil Drag Force (N)	Modified Airfoil Drag Force (N)
20	35.79	1.5	2.75	1.5
30	51.45	4.5	4.5	2.75
40	67.11	7	8	5
50	78.29	12.5	12.5	9
60	111.85	18	17.5	14.5

3.4 Roll Bar Testing

The roll bar was too large to insert into a universal testing machine without custom fittings, so we decided to resort to manual testing. We loaded the roll bar with 2 individuals with a combined weight of 350 pounds. As a result of the stress of the combined load, the roll bar fractured at the location which the analysis showed was weakest. The problem was not due to the material, but rather was a function of the construction. To rectify this problem we will rebuild the roll bar with the same material but more meticulous construction by competition time.

3.5 Seat Testing

It was important to determine the proper head angle for the highest degree of comfort and visibility. To determine this optimum angle, riders were asked to sit on the seat and position their head as needed to be most comfortable. This angle (between the plane of the seat back and the middle of the neck) was determined to be consistently between 40 and 50 degrees. In order to maintain this position, a special wedge pillow will be used to cushion the head. The perpendicular distance between the ear and the back of the seat was also measured in order to establish another possible correlation between rider height, rider position, and head angle. After numerous data points, it was determined that this data was irrelevant and there was not a correlation of any type. This average distance was measure to be about eight inches.

4 Safety

For a human powered vehicle, safety is an important consideration for both the rider as well as bystanders. To this effect, we have considered six key aspects of the bicycle to determine its safety.

Shell

The shell consists of three main components: a thermoformed PETG window, a fiberglass composite nosecone, and a fiberglass reinforced Coroplast body section. There are no sharp edges on the inside or outside of the structure. For the endurance event, the nosecone has been modified to allow the rider to put down his or her feet to prevent the vehicle from falling over and facilitate rider changes. The shell is firmly and elastically connected to the frame to prevent it from malfunctioning during competition and potentially becoming a hazard.

Frame

The frame was manufactured out of steel to take advantage of its high strength and fatigue resistance. In cases of massive, sudden loading, a steel frame will only deform, rather than failing catastrophically as an aluminum frame might.

Seat Belt

The seat will include a four-point harness racing seat belt made of 2in heavy duty nylon straps.

Roll Over and Side Protection

A roll bar is securely attached to the frame of the vehicle and surrounds the rider's entire body with helmet and pedal path so that it is the first part of the bike to hit the ground. It is located at the head of the rider to maximize shoulder protection.

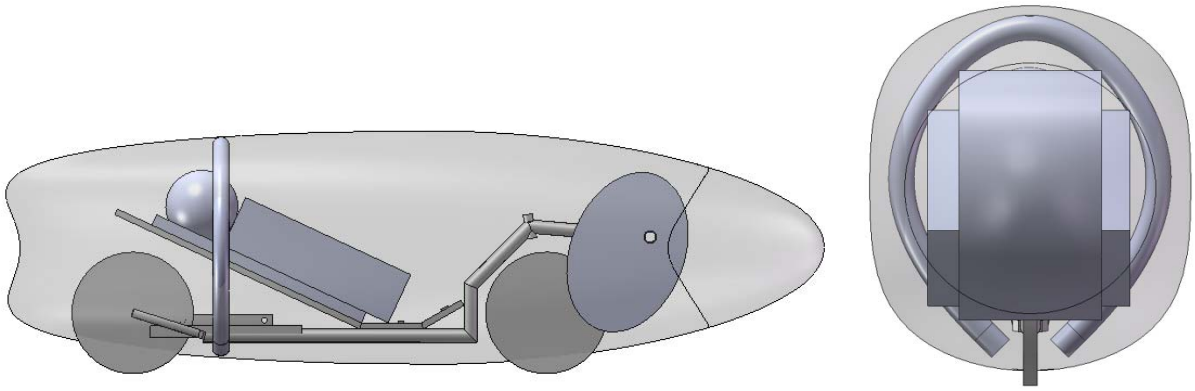

Figure 26. The roll bar is placed at the head of the rider and surrounds the shoulders as well as the pedal path.

The nosecone window is made out of PETG, a strong, impact-resistant material. The roll bar is made of a fiberglass-carbon hybrid composite with three layers (fiberglass, carbon, and fiberglass) to capitalize on the materials properties of both. Fiberglass has a higher abrasion resistance than carbon fiber so there is a thin layer of fiberglass on the outermost part of the roll bar. The inner carbon layer serves to increase the strength and energy absorption of the roll bar with minimal additional weight. The Coroplast body also offers side-protection and resists tearing.

Visibility

This year, we have greatly improved the rider's visibility by thermoforming a large PETG window that encompasses half of the nosecone. Since our design requires the rider's head to be below his or her knees, the rider's vision is obstructed periodically by the rotation of the legs with the pedals as well as partially by the steering mechanism. However, as evidenced by our performance last year, it is clearly possible to adjust to these small obstructions. The window continues into the Coroplast body to maximize the peripheral view.